JMEPEG (2011) 20:409–416
DOI: 10.1007/s11665-010-9692-3

1059-9495/$19.00

Corrosion Behavior of Mild Carbon Steel in Ethanolic Solutions

Shaily M. Bhola, Rahul Bhola, Luke Jain, Brajendra Mishra, and David L. Olson

(Submitted November 17, 2009; in revised form March 30, 2010)

Electrochemical evaluation of ASTM A36 steel was performed in ethanolic solutions containing small concentrations of water ranging from 0 to 10 vol.%. Electrochemical techniques such as open circuit potential (OCP), electrochemical impedance spectroscopy (EIS), and potentiodynamic polarization were utilized to analyze corrosion parameters. A fixed concentration of chloride, as per the ASTM specification for fuel grade ethanol, was added to increase the conductivity of the solutions. The effects of water and oxygen on the corrosion behavior of steel in these solutions have been discussed. Pitting corrosion of the steel specimens in these solutions was evaluated using scanning electron microscopy (SEM) and pitting analysis. This investigation was performed to establish a baseline for the microbiologically influenced corrosion (MIC) of steel in ethanolic solutions.

Keywords corrosion, EIS, ethanolic solutions, mild carbon steel

1. Introduction

The corrosion of transportation infrastructure for fuel grade ethanol and ethanol fuel blends has been a major concern. Various service failures have been reported, especially relating to the ethanol stress corrosion cracking (eSCC) of mild carbon steel in ethanolic environments (Ref 1, 2). Laboratory studies have evaluated environmental constituents including dissolved oxygen and chloride which have been shown to increase the susceptibility of steel to SCC (Ref 3-6). The possibility of microbiologically influenced corrosion (MIC) affecting these facilities and increasing the propensity toward localized corrosion forms such as SCC and pitting corrosion is being realized.

The aim of this investigation is to understand the roles of water and oxygen concentrations in ethanolic solutions on the corrosion of stressed mild carbon steel and to serve as a benchmark for the MIC investigation (Ref 7), since MIC is considered an enhancer to the traditional forms of corrosion. Plastic deformation was induced to mild carbon steel to provide preliminary understanding on the effects of strain on electrochemical properties. Localized differentials in strain within a material can give local differentials in electrochemical potential. Microcracks on the specimen surface, resulting from deformation, can allow for the creation of localized cells on the metal in contact with the solution at the micro-environmental level. The electrochemical properties of the deformed specimen can thus be widely different from those of an unloaded specimen. There have been reports (Ref 4, 5) on the use of various electrochemical techniques to evaluate the corrosion chemistry of steel in ethanolic solutions. However, to our knowledge, the use of electrochemical impedance spectroscopy (EIS) to investigate interfacial properties of steel in ethanolic solutions was not found in the literature at the time when this investigation was started. This study incorporates the use of EIS on the corrosion behavior of steel in ethanolic solutions.

Shaily M. Bhola, Rahul Bhola, Luke Jain, Brajendra Mishra, and **David L. Olson**, Department of Metallurgical and Materials Engineering, Colorado School of Mines, Golden, CO 80401. Contact e-mail: sbhola@mines.edu.

2. Experimental

2.1 Materials Preparation and Test Set-Up

The ASTM grade A36 steel (Ref 8) with composition as shown in Table 1 was used for the investigation. Steel U-bends were prepared according to the ASTM standard (Ref 9). Rectangular specimens 0.07 in. were machined to 5 in. × 0.76 in. The specimens were given a surface finish of 12-17 R_a. These were then severely plastically deformed into U-bends and fixed with a bolt.

In order to utilize the U-bends as working electrodes for electrochemical measurements, a copper wire was crimped into a ring terminal, which was slid around the loading bolt and pressed between the loading nut and one side of the specimen. The specimen was oriented with the most highly stressed area faced down. A surface area of 16 cm^2 was immersed in solution, while the remaining non-immersed part of the specimen was coated to avoid the galvanic corrosion between the specimen and the loading nut and bolt or the copper wire which may occur due to the condensation of solution vapors in the closed system used for the investigation. A non-aqueous Ag/AgCl/EtOH/LiCl electrode was used as a reference electrode, and a platinum wire was used as a counter-electrode. The potential of the reference electrode was 0.097 V with respect to Normal Hydrogen Electrode (N.H.E.). A glass cell with ports equipped with stoppers for the three electrodes (working, reference, and counter) and purge tubes (for purging with oxygen and nitrogen) was employed for the study.

Table 1 Chemical composition in wt.% for ASTM A-36 steel as determined by OES

C	S	P	Si	Cr	Ni	Mn	Cu	Mo	Nb	Ti	Al	V	Co	W
0.22	0.008	0.014	0.04	0.08	0.08	0.9	0.23	0.02	<0.01	<0.01	0.03	<0.01	<0.01	<0.01

Experimental solutions included 200 proof absolute ethanol and 200 proof absolute ethanol containing 1, 3, 5, 7, and 10 vol.% water. A chloride solution of 19.4 mg L^{-1} in the form of NaCl was added to solutions of ethanol and water to increase the conductivity of these solutions. Electrochemical measurements were performed on the U-bend specimens immersed in these solutions under different levels of aeration: deaerated (by purging with N_2), under static air, and aerated (by purging with O_2) at 298 K.

2.2 Measurements

2.2.1 Electrochemical Techniques. For performing various electrochemical techniques on the system, a PAR Potentiostat 273A and a PAR 1255 FRA were used.

Open circuit potential (OCP): The OCP values of the U-bends immersed in the above solutions at different aeration levels were monitored with time during the immersion period of upto 48 h.

Electrochemical impedance spectroscopy (EIS): The impedance measurements were performed at the OCP for various immersion intervals such as immersion, 2, 6, 12, 24, 36, and 48 h. The frequency sweep was applied from 10^5 to 10^{-2} Hz with the AC amplitude of 10 mV.

Potentiodynamic polarization: After an immersion interval of 48 h, a potentiodynamic polarization sweep was applied to the system by polarizing the working electrode from an initial potential of −500 mV versus the OCP, upto a final potential of 2 V. The ASTM standard scan rate of 0.1667 mV/s (Ref 10) was used for the polarization sweep. The ohmic compensation was applied by performing EIS measurements after the polarization experiments and using the value of solution resistance from the impedance response to modify the polarization curves generated.

2.3 Scanning Electron Microscopy

The SEM imaging was performed on the specimens using a FEI Quanta 600 scanning electron microscope after 48 h of immersion in various solutions under static air conditions to evaluate the pitting behavior of mild carbon steel. Before performing the SEM and pitting analyses, the specimens were cleaned to remove the corrosion products as per ASTM standard (Ref 11).

2.4 Pitting Analysis

The evaluation of the pit depth and pit size was performed for a detailed analysis of the nature of pits formed on these specimens using the procedure defined by ASTM (Ref 12).

3. Results and Discussion

Figure 1-3 show the OCP variation as a function of time for mild carbon steel in different ethanolic solutions under deaerated, static air, and oxygen-purged conditions. The OCP

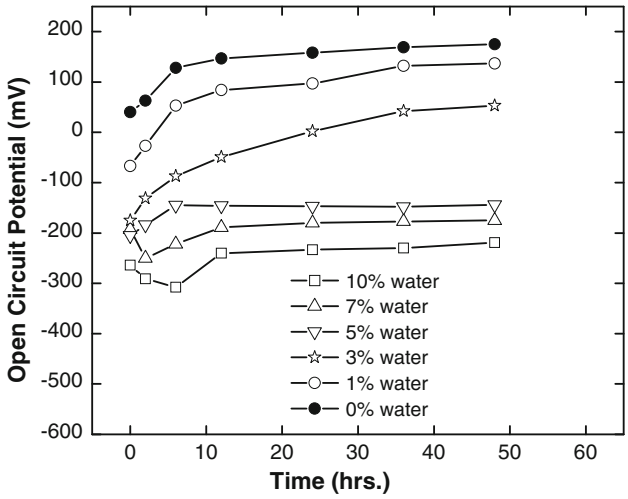

Fig. 1 OCP values as a function of time for ASTM A36 steel immersed in ethanol with varying water concentrations under deaerated conditions at 298 K (all but 0 vol.% water containing solution contain 19.4 mg L^{-1} Cl^-)

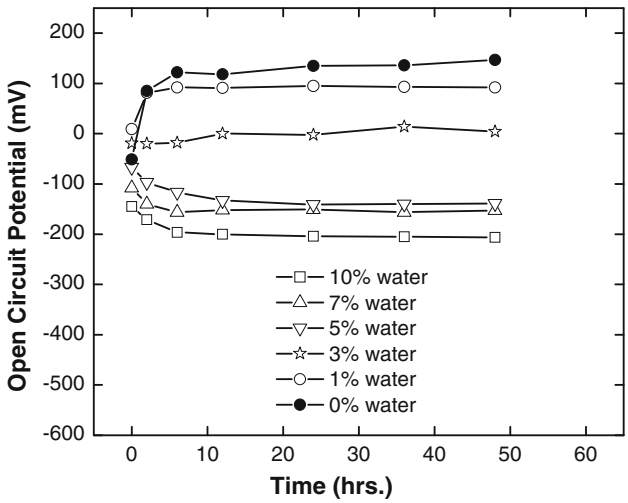

Fig. 2 OCP values as a function of time for ASTM A36 steel immersed in ethanol with varying water concentrations in static air at 298 K (all but 0 vol.% water containing solution contain 19.4 mg L^{-1} Cl^-)

values are the most noble for pure ethanol, and the least noble (most active) for the solution containing the highest concentration of water. All the intermediate solutions follow a trend in the same order.

The 0 vol.% water solution corresponds to pure ethanol without any addition of the chloride ions. The steel specimens immersed in this solution offer high resistance to the charge transfer taking place on the steel surface as seen from the noble OCP values for such a case. Solutions with water ranging from

1 to 10 vol.% contain 19.4 mg L^{-1} of the added chloride, which is within ASTM specifications for the fuel grade ethanol (Ref 13). Water added to ethanol upto 1 vol.% is again within ASTM limits (Ref 13), and the OCP values for such a case are very close to the OCP values for pure ethanol. The OCP curves for the solutions with 0, 1, and 3 vol.% water are quite separated from the curves for solutions with 5, 7, and 10 vol.% water for all the three aeration conditions in Fig. 1-3. This separation increases as the level of aeration is increased. In the former case, the OCP values show an initial increase, and in the latter case, there is an initial decrease in the OCP values for all the three levels of aeration. The increase or decrease in the OCP values is observed to show a significant change only in the first 6 h from immersion. The initial increase in the OCP values in the former case indicates the thermodynamic stability of steel in these solutions. However, a decrease in OCP values in the latter case is due to the increased charge transfer taking place on the steel surface due to increased water concentrations. As will also be mentioned later, no rust was evident on the specimens immersed in solutions with 0 to 3 vol.% water during the initial 6 h after immersion. On the other hand, rust was observed in just 2 h upon immersion in solutions with 5-10 vol.% water. It is also observed in Fig. 1-3 that the OCP values become nobler with increasing oxygen concentration. However, the OCP increase with increasing oxygen concentration is less than that with decreasing water concentrations.

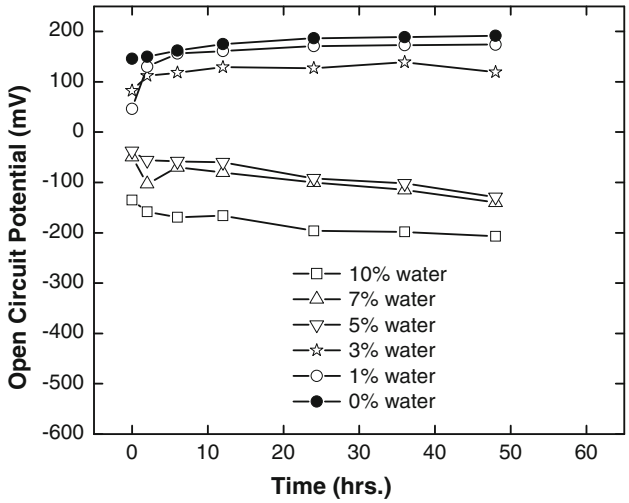

Fig. 3 OCP values as a function of time for ASTM A36 steel immersed in ethanol with varying water concentrations under oxygen-purged conditions at 298 K (all but 0 vol.% water containing solution contain 19.4 mg L^{-1} Cl^{-})

On visual inspection of the steel specimens immersed in various solutions in static air, no rust was observed for ethanol with 0 vol.% (containing no chloride) and 1 vol.% (containing 19.4 mg L^{-1} chloride) water even upto 48 h of immersion. Very little rust was observed for ethanol with 3 vol.% water, but only after 24 h of immersion. For ethanol containing 5-10 vol.% water, rust was observed within just 2 h of immersion. Figure 4(a) shows an un-pitted specimen after 48 h of immersion in ethanol with 1 vol.% water. Figure 4(b), on the other hand, shows an extensive rust and pits on the specimen immersed for the same time duration in ethanol with 7 vol.% water.

The SEM imaging was performed on the specimens immersed for 48 h in solutions with varying water concentrations under static air conditions. Deaerated and oxygen-purged conditions did not exhibit much variation with regard to the pitting morphology of pits, and hence have not been shown. Detailed electrochemical analysis on the effect of aeration has been included in the later part of this article. Neither rust nor pitting was observed for ethanol containing 0 and 1 vol.% water. Extensive pitting was observed for specimens immersed in solutions with water ranging between 3 and 10 vol.% With the concentration of chloride ions being equivalent (19.4 mg L^{-1}) in all these cases, the extent of pitting varied with respect to the water content. Figure 5 shows the SEM micrographs of the specimens with pits.

Figure 6 shows the SEM images at higher magnifications for a pit covered with corrosion products, present on a specimen immersed in ethanol with 7 vol.% water.

Table 2 shows the pit parameters for the pits shown in Fig. 5. The average pit depths for the pits on the specimens immersed in solutions with 3-7 vol.% water are almost similar and slightly greater than the average pit depth corresponding to 10 vol.% solution. The average pit diameters are close for solutions with 3 and 5 vol.% water but, thereafter, increase with increase in the water content. As known so far from the

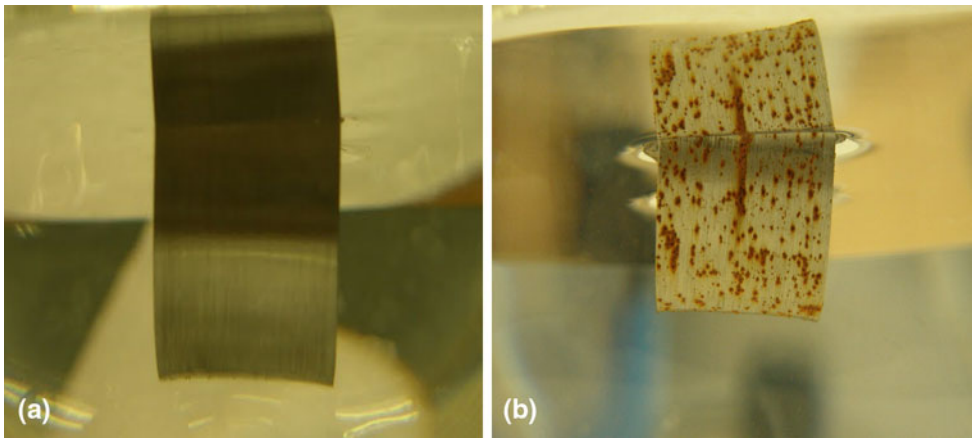

Fig. 4 U-bend specimens immersed for 48 h. under static air conditions at 298 K in ethanol with (a) 1 vol.% water and (b) 7 vol.% water, each containing 19.4 mg L^{-1} Cl^{-}

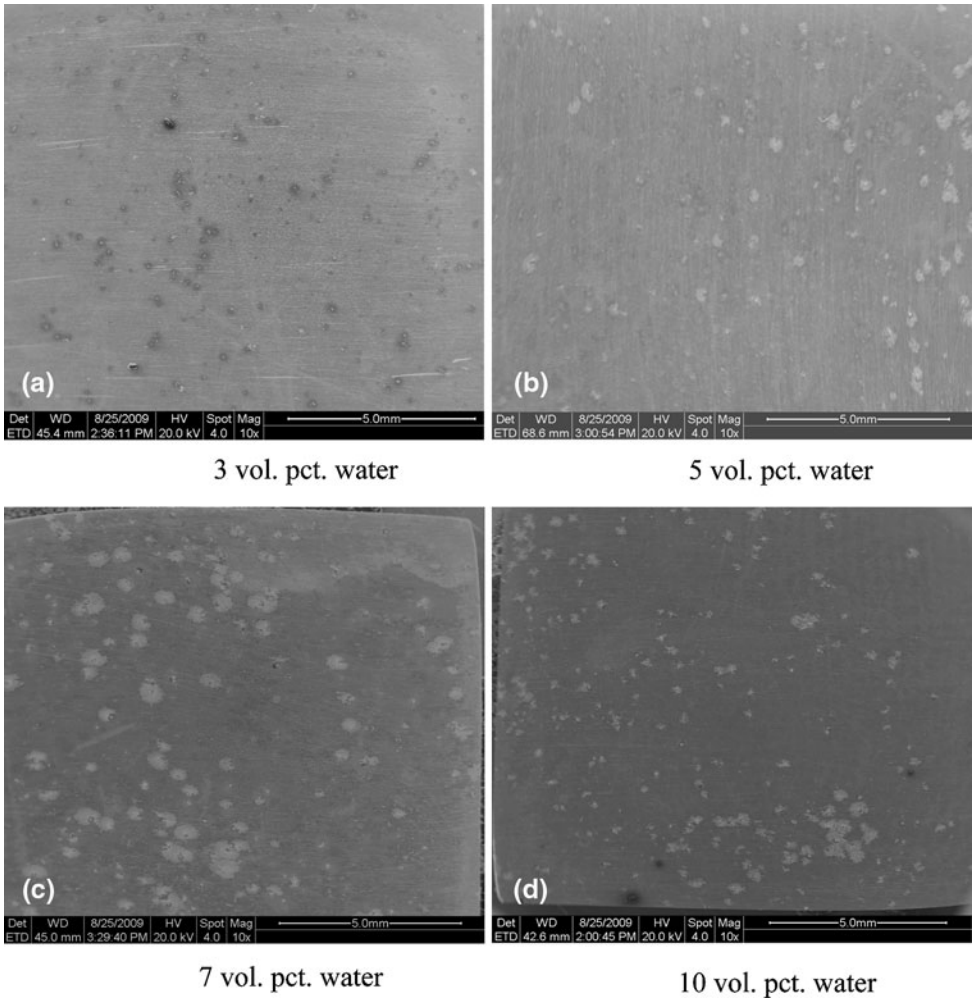

Fig. 5 SEM micrographs at 10× magnification of ASTM A36 steel specimens immersed for 48 h in ethanol with varying water concentrations and 19.4 mg L^{-1} Cl^{-} under static air conditions at 298 K

behavior of open circuit potentials and as will also be seen in the EIS and potentiodynamic results, water plays an important role in increasing the propensity of steel toward corrosion. Pitting analysis indicates that increasing the water content in ethanol results in increasing the pit size and decreasing the pit depth. This phenomenon can be comprehended as a transition from a localized corrosion to a uniform corrosion with increasing water additions. The values of roughness parameters, R_a (the arithmetic average of the absolute height values of all points of the profile) and R_q (the root mean square of the values of all points of the profile) show an increase with increasing water concentrations, indicating an increase in the extent of corrosive attack. Wolynec and Tanaka (Ref 14) also observed that in acidified ethanol solutions, low concentrations of water lead to a dramatic decrease in general corrosion and onset of pitting at around 4% water in ethanol. Higher additions of water promoted uniform (general) corrosion.

Figure 7 and 8 show the variation of polarization resistance (R_p) and double layer capacitance which is represented by constant phase element (CPE) with time for steel specimens in various solutions under static air conditions. These values have been derived from EIS circuit modeling, and the methodology adopted for the fitting procedure has been discussed in the next section. The R_p-time plot appears similar to the OCP-time plot for the static air condition, with solutions containing lower concentrations of water showing nobler OCP (more positive) as well as higher R_p values and vice versa. Curves for these solutions under deaerated and oxygen-purged conditions showed similar trends to the respective OCP-time curves and hence have not been shown. The capacitance-time plot shows an exactly reverse trend to the R_p-time plot. The dielectric constant of water (77.9 at 298 K) is higher than that of ethanol (24.3 at 298 K) because of its higher polarity. Its conductivity is also an order of magnitude higher than that of ethanol. Owing to these properties, ethanolic solutions with increasing concentrations of water show higher double layer capacitance values and lower polarization resistance values, in other words, they show higher corrosion rates.

Figure 9 shows a variation in R_p as a function of vol.% water added to ethanol under different aeration conditions after 2 h of immersion. The R_p values follow the order: R_p (oxygen purged) < R_p (static air) < R_p (deaerated) for all solutions. The order observed was similar for other immersion times. Water appears to be a more important parameter in increasing the susceptibility of steel to corrosive attack when compared to oxygen, as varying the amount of water produces a more significant change in R_p values over decades of magnitude, compared to which oxygen produces a small change.

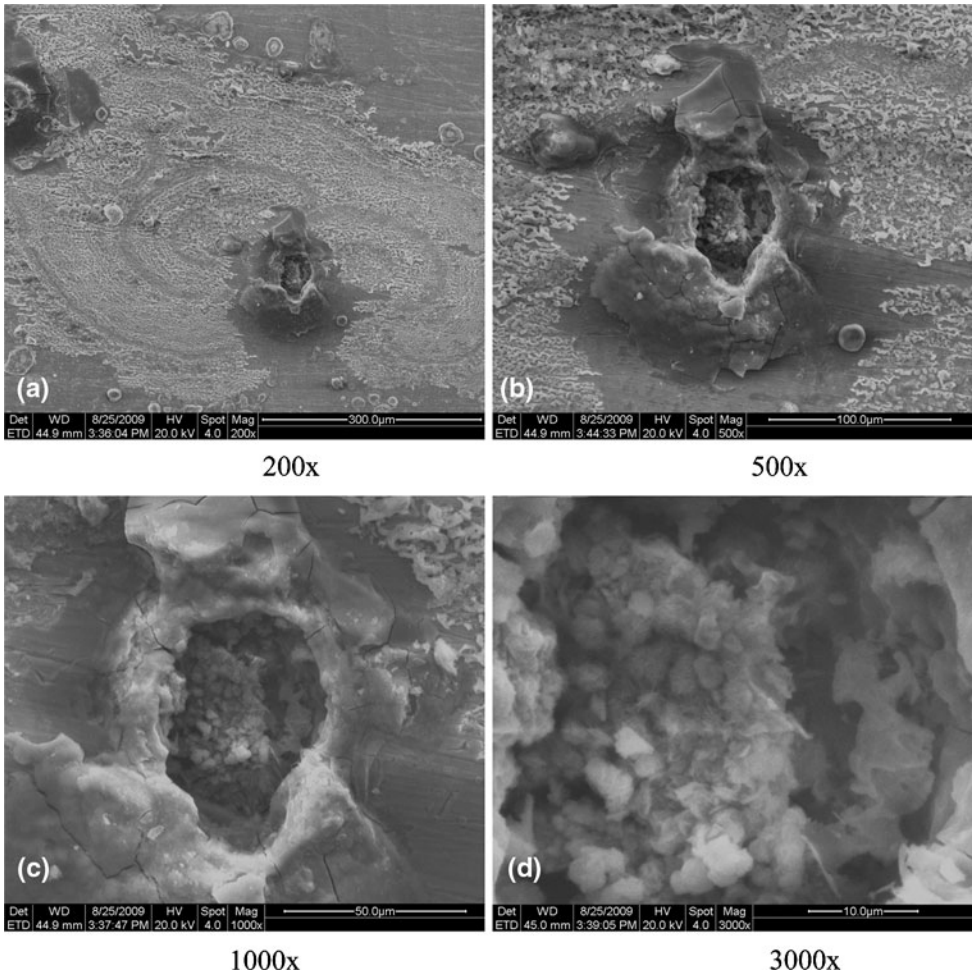

Fig. 6 SEM micrographs at higher magnifications of a pit present on the ASTM A36 steel specimen immersed for 48 h in ethanol containing 7 vol.% water and 19.4 mg L^{-1} Cl^- under static air conditions at 298 K

Table 2 Pit parameters for ASTM A36 steel in various ethanolic solutions, each containing 19.4 mg L^{-1} Cl^-, after 48 h of immersion under static air conditions at 298 K

Water, vol.%	Average pit depth, µm	Average pit diameter, µm	Pit diameter of the largest pit, µm	R_a, µm	R_q, µm
3	28.88	20.19	23.03	3.90	4.51
5	28.95	20.60	25.40	4.52	5.21
7	29.08	30.29	32.40	4.59	5.25
10	26.54	35.66	42.17	5.27	6.05

R_a = Arithmetic average of the absolute height values of all points of the profile; R_q = Root mean square of the values of all points of the profile

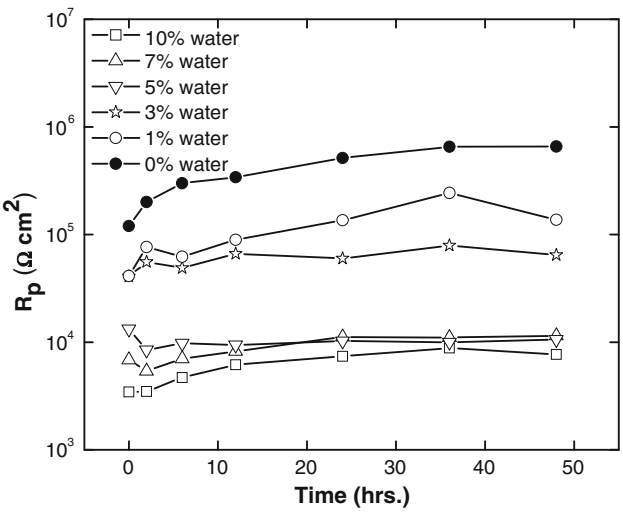

Fig. 7 Polarization resistance as a function of time for ASTM A36 steel immersed in various solutions in static air at 298 K (all but 0 vol.% water containing solution contain 19.4 mg L^{-1} Cl^-)

Figure 10 shows the EIS Bode plots for steel immersed for 48 h in ethanol with 10 vol.% water under different aeration conditions. Figure 11 shows the EIS Bode plots for the steel immersed for 48 h in ethanol with 0, 3, and 10 vol.% water under static air conditions.

In low conductivity media, higher frequencies usually exhibit artifacts which may take form of capacitive or inductive arcs connected with loops (Ref 15, 16). These artifacts may be misinterpreted as interfacial properties. Investigators have attributed these artifacts to parasitic conduction paths within

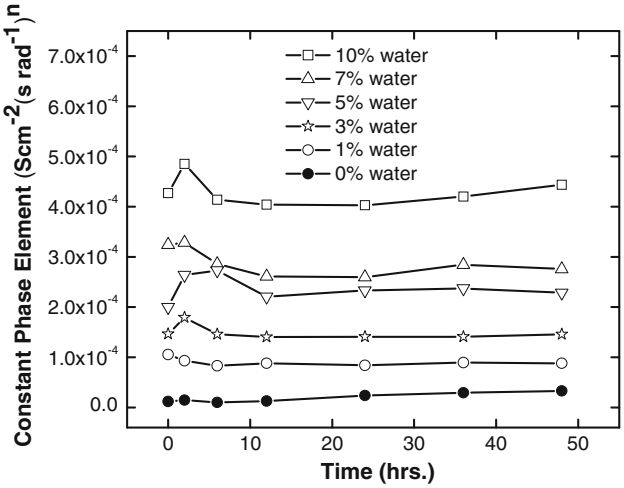

Fig. 8 Double layer capacitance as a function of time for ASTM A36 steel immersed in various solutions in static air at 298 K (all but 0 vol.% water containing solution contain 19.4 mg L^{-1} Cl^{-})

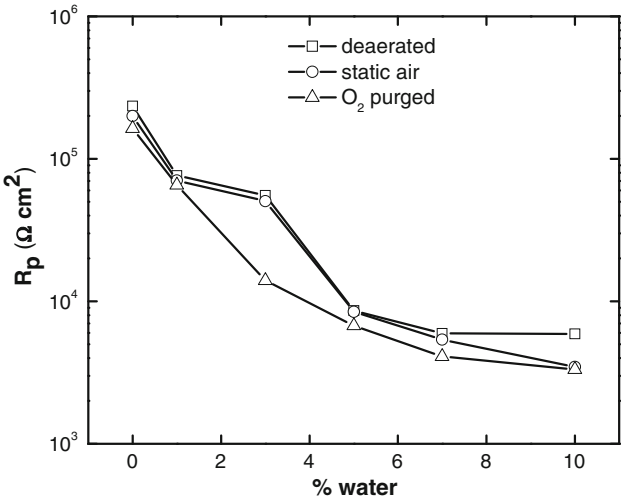

Fig. 9 Variation of polarization resistance with vol.% water for ASTM A36 steel at 2 h of immersion under different levels of aeration at 298 K (all but 0 vol.% water containing solution contain 19.4 mg L^{-1} Cl^{-})

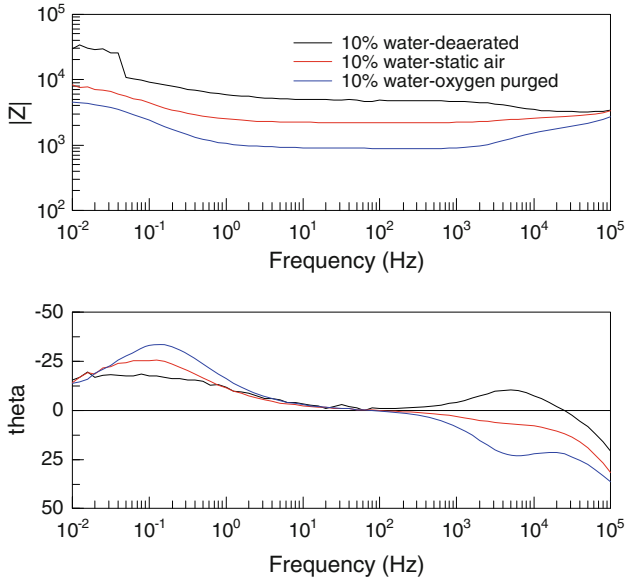

Fig. 10 EIS Bode plots for ASTM A36 steel immersed for 48 h in ethanol with 10 vol.% water and 19.4 mg L^{-1} Cl^{-} under different levels of aeration at 298 K

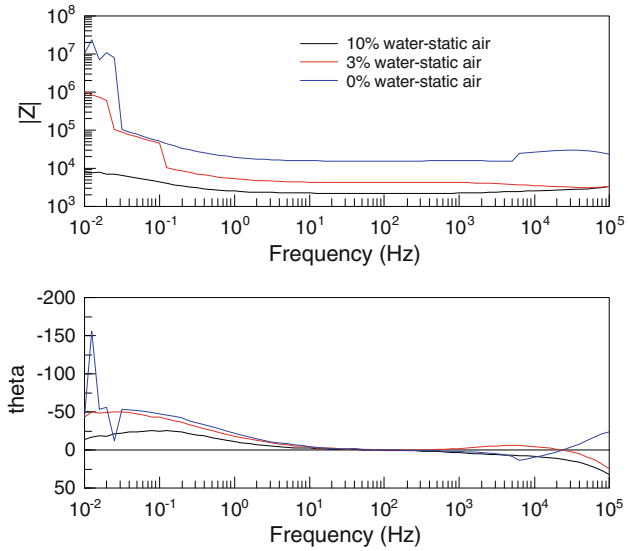

Fig. 11 EIS Bode plots for ASTM A36 steel immersed for 48 h in ethanol with different vol.% water in static air at 298 K (all but 0 vol.% water containing solution contain 19.4 mg L^{-1} Cl^{-})

the electrochemical cell and the measurement system. These are due to the interference caused by measurement electronics, electrochemical cell (geometry, reference, wiring, and connections), and high solution resistance (Ref 15). In order to analyze the EIS curves generated in this study, those data above 100 Hz were considered artifactual, and those within the frequency range 100-0.01 Hz were used to extract interfacial information.

It can also be observed from Fig. 10 and 11 that the phase angle approaches 0° and remains close to 0° at around 100 Hz over a relatively wide frequency range compared to some other parts in the artifactual high frequency regions, which also cross through 0°. Therefore, the value of the impedance modulus corresponding to this wide frequency range was taken as the solution resistance. The data in the 100-0.01 Hz frequency range were found to fit the circuit model shown in Fig. 12(a) where Rs is the solution resistance; R1, the polarization resistance; and CPE1, the constant phase element, used to represent the double layer capacitance (Ref 17). Impedance of the CPE is given by,

$$Z(\mathrm{CPE}) = [Q(j\omega)^n]^{-1}$$

where Q is the constant of CPE, and ω is the angular frequency in rad s^{-1}.

For a capacitor, $n = 1$, and for a CPE, n varies as $-1 \leq n \leq 1$. $n\pi/2$ represents the constant phase angle of the CPE in radians.

In some cases, a diffusion impedance (Z_D) represented by W1, Warburg coefficient, was found to be present in addition to

Fig. 12 Circuit models used to fit EIS results

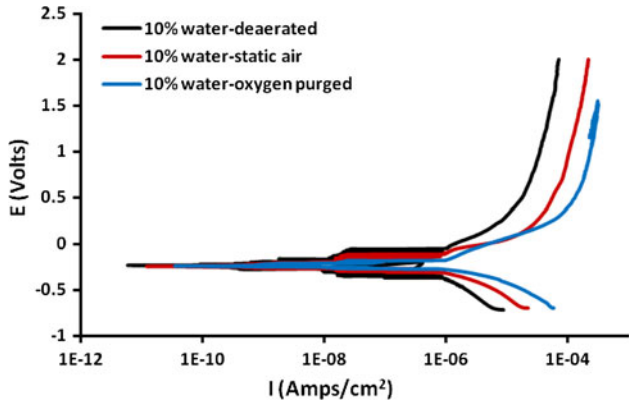

Fig. 13 Potentiodynamic polarization curves for ASTM A36 steel immersed for 48 h in ethanol with 10 vol.% water and 19.4 mg L^{-1} Cl^- under different levels of aeration at 298 K

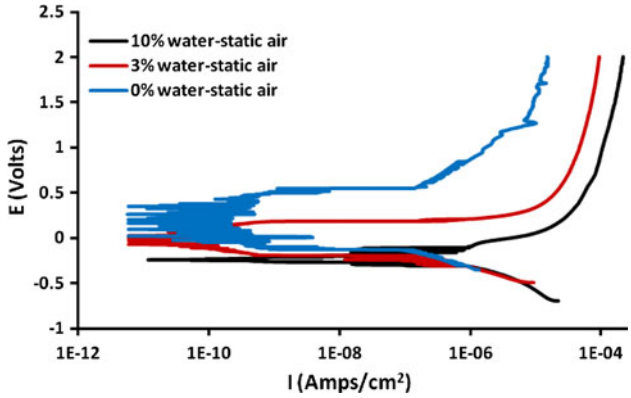

Fig. 14 Potentiodynamic polarization curves for ASTM A36 steel immersed for 48 h in ethanol with different vol.% water in static air at 298 K (all but 0 vol.% water containing solution contain 19.4 mg L^{-1} Cl^-)

Table 3 Corrosion parameters for ASTM A36 steel immersed for 48 h in various ethanolic solutions at 298 K

		Corrosion current density ($\times 10^{-7}$), A/cm^2			Corrosion potential, V		
Water, vol.%	Conc. of Cl^-, mg L^{-1}	Deaerated	Static air	O_2 purged	Deaerated	Static air	O_2 purged
0	0	0.10	0.24	0.25	0.147	0.175	0.192
1	19.4	0.34	0.39	2.46	0.092	0.137	0.174
3	19.4	0.45	0.48	6.42	0.004	0.053	0.119
5	19.4	2.42	4.05	12.42	−0.144	−0.139	−0.129
7	19.4	2.74	6.88	23.09	−0.175	−0.153	−0.140
10	19.4	7.75	10.50	25.96	−0.219	−0.207	−0.205

the charge transfer resistance, R1, and the data fitted the circuit shown in Fig. 12(b). In such a case, R_p = R1 + Z_D.

In Fig. 10, it can be seen from the low frequency end of the spectrum that the impedance values are the highest for the deaerated condition, followed by static air and lowest for oxygen purged. The peaks of the phase angle in the 100-0.01 Hz frequency range show an inverse order. These observations are in agreement with the changes observed in the corresponding potentiodynamic polarization curves under these conditions in Fig. 13. The different degrees of aeration seem to have affected both the cathodic and anodic current densities in the active region and also the passivation current density values, with the highest current densities being observed for the oxygen-purged condition, followed by those for static air, and those for deaerated.

From Fig. 11, it can be seen that the steel immersed in solutions with higher water concentrations at similar aeration levels shows lower impedance modulus values at the low frequency end of the spectrum, suggesting lower corrosion rates. Potentiodynamic curves for solutions under similar conditions, as shown in Fig. 14, reveal that with varying water concentration, the cathodic current densities are neither shifted nor do they show a change in cathodic slope. Anodic current densities (both active and passive regions), on the other hand, are significantly affected. This increase in the anodic current densities with increasing water additions to ethanol result in the shift in corrosion potentials towards the active direction.

Table 3 lists the corrosion parameters for A36 steel in various ethanolic solutions discussed so far. The corrosion current density values increase with increasing aeration and increasing water content, in accordance with the observations made above.

4. Conclusions

1. The OCP values for ASTM A36 steel in various ethanolic solutions with a fixed concentration of chloride and varying concentrations of water, decrease with increasing the additions of water. The shift in the active direction is due to the increase in the charge transfer occurring on the steel surface in the presence of water. The polarization resistance (from EIS analysis) also shows a decrease

with increasing water additions, and the double layer capacitance shows an exactly reverse trend.
2. Visual inspection and SEM analysis under static air conditions revealed the presence of rust and pits on the steel specimens in solutions with water concentration in the range 3-10 vol.% No rust and pits were observed in the presence of 1 and 0 vol.%, even up to 48 h of immersion.
3. Pitting analysis indicates that increasing the water concentration in ethanol results in an increase in pit size which is due to the transition from localized corrosion to uniform corrosion.
4. R_p values for steel seem to be affected by the presence of oxygen in the order: R_p (oxygen purged) $< R_p$ (static air) $< R_p$ (deaerated) for all solutions. The effect of water is more significant than oxygen in increasing the charge transfer kinetics of steel. Different degrees of aeration seem to have affected both the cathodic and anodic current densities in the active region of the Tafel curves and also the passivation current densities, with the highest current density being for the oxygen-purged condition, followed by static air and then deaerated.
5. The effect of increasing water concentrations on the Tafel behavior shows that the cathodic current densities are unaffected by the increasing amounts of water, as compared to the anodic current densities (both active and passive regions), which are highly affected by the addition of water. The significant increase in the anodic current densities observed with increasing amounts of water to ethanol result in the shift in corrosion potentials towards the active direction.

Acknowledgments

The authors acknowledge and appreciate the support of the U.S. DOT-PHMSA, the U.S. DOC-NIST, and the American Bureau of Shipping. The authors further acknowledge the help offered by Hussain H. Obaid for this study.

References

1. C.A. Farina and U. Grassini, Stress Corrosion Cracking in Non-Aqueous Media, *Electrochim. Acta*, 1987, **32**, p 977–980
2. R.D. Kane and J.G. Maldonado, Stress Corrosion Cracking in Fuel Ethanol: A Newly Recognized Phenomenon, *Corrosion*, 2004; NACE, Paper No. 04543
3. R.D. Kane, N. Sridhar, M.P. Brongers, J.A. Beavers, A.K. Agrawal, and L.J. Klein, Stress Corrosion Cracking in Fuel Ethanol: A Recently Recognized Phenomenon, *Mater. Perform.*, 2005, **44**(12), p 50–55
4. N. Sridhar, K. Price, J. Buckingham, and J. Dante, Stress Corrosion Cracking of Carbon Steel in Ethanol, *Corrosion*, 2006, **62**(8), p 687–702
5. J.G. Maldonado and N. Sridhar, SCC of Carbon Steel in Fuel Ethanol Service: Effect of Corrosion Potential and Ethanol Processing Source, *Corrosion*, 2007; NACE, Paper No. 07574
6. R.C. Newman, Review and Hypothesis for the Stress Corrosion Mechanism of Carbon Steel in Alcohols, *Corrosion*, 2008, **64**(11), p 819–823
7. L. Jain, C. Williamson, S.M. Bhola, R. Bhola, J.R. Spear, B. Mishra, D.L. Olson, and R. Kane, Microbiological and Electrochemical Evaluation of Corrosion in Microbiologically Influenced Corrosion of Steel in Ethanol Fuel Enviornments. *Proceedings of NACE Corrosion 2010 Conference*, NACE International, USA
8. ASTM Standard A36/A36 M, *Standard Specification for Carbon Structural Steel*, ASTM International, USA, 2008
9. ASTM Standard G 30-97, *Standard Practice for Making and Using U-Bend Stress Corrosion Test Specimens*, ASTM International, USA, 2009
10. ASTM Standard G 5-94, *Standard Reference Test Method for Making Potentiostatic and Potentiodynamic Anodic Polarization Measurements*, ASTM International, USA, 2004
11. ASTM Standard G 1, *Standard Practice for Preparing, Cleaning and Evaluating Corrosion Test Specimens*, ASTM International, USA, 2003
12. ASTM Standard G 46-94, *Standard Guide for Examination and Evaluation of Pitting Corrosion*, ASTM International, USA, 2005
13. ASTM Standard D 4806, *Standard Specification for Denatured Fuel Ethanol for Blending with Gasolines for Use as Automotive Spark-Ignition Engine Fuel*, ASTM International, USA, 2001
14. S. Wolynec and D.K. Tanaka, *Corrosion in Ethanol Fuel Powered Cars: Problems and Remedies*, IPT, Sao Paulo, SP, Brazil, p 464–474
15. K.C. Stewart, D.G. Kolman, and S.R. Taylor, The Effect of Parasitic Conduction Pathways on EIS Measurements in Low Conductivity Media, *Electrochemical Impedance: Analysis and Interpretation*, ASTM STP 1188, J.R. Scully, D.C. Silverman, and M.W. Kendig, Ed., American Society for Testing and Materials, Philadelphia, 1993, p 73–93
16. S. Chechirlian, M. Keddam, and H. Takenouti, Specific Aspects of Impedance Measurements in Low Conductivity Media, *Electrochemical Impedance: Analysis and Interpretation*, ASTM STP 1188, J.R. Scully, D.C. Silverman, and M.W. Kendig, Ed., American Society for Testing and Materials, Philadelphia, 1993, p 23–36
17. R.G. Kelly, J.R. Scully, D.W. Shoesmith, and R.G. Buchheit, *Electrochemical Techniques in Corrosion Science and Engineering*, Marcel Dekker, Inc, New York, USA, 2003, p 125–150